# Photonic Band Gap Analysis of Silicon Photonic-Crystal Slab Structures with Non-Circular Air Holes

L. Kassa-Baghdouche*

*Department of Electronics and Telecommunications, Faculty of Science and Technology, 8 May 1945 University of Guelma, 24000 Guelma, Algeria*

Received: 10.01.2020 & Accepted: 20.05.2020

Doi: 10.12693/APhysPolA.138.421 *e-mail: kassabaghdouche_lazhar@yahoo.com

In the present study, analysis of photonic band gap properties of silicon photonic crystal slab structures composed of non-circular air holes was performed. In order to estimate the design of the opto-geometrical parameters for maximizing the photonic band gap, three structures have been proposed and analyzed in the present study. These three structures comprised elliptical, rectangular, and hexagonal air holes in a triangular lattice. The band diagrams of electromagnetic waves and photonic band gap properties of the proposed structures were determined using three-dimensional supercell plane-wave expansion method. The results obtained indicated that the photonic band gaps for the transverse electric polarized modes were larger for the structure composed of hexagonal air holes, while the photonic band gaps were low for the structures composed of elliptical and rectangular air holes. Furthermore, it was demonstrated that the photonic band gaps of the proposed structures are altered with variation in the rotation angle of their constituent air holes. These findings suggested that the proposed silicon photonic crystal slab structures presented significantly large photonic band gaps, and therefore, served as a promising technology platform for designing photonic crystal cavities and waveguides.

topics: photonic crystal slab (PhC), non-circular air holes, photonic band gap, 3D supercell plane-wave expansion method

## 1. Introduction

Several years of great efforts have been devoted to the study of photonic crystals (PhC) because of their unique electromagnetic properties and potential applications in the fields of optoelectronics and optical communications [1, 2]. The most important property of the PhC structures is the photonic band gap (PBG), which represents the presence of a frequency spectrum region in which the propagation of light is forbidden [3, 4]. Photonic band gaps in a PhC structure play a vital role in the realization of photonic devices, and a large photonic band gap is required for the various applications of such structures, for example in defect mode PhC lasers, high-Q point-defect PhC nanocavities, slotted PhC waveguides and mid-infrared sensors [5–15].

Recently, several researchers have proposed engineering the photonic band gap of photonic crystals. Matthews et al. [16] reported band gap engineering of two-dimensional photonic crystals (2D-PhCs) constituting of a triangular lattice containing rotated hexagonal holes. The effects of reduced symmetry in the unit-cell geometry on the band gap and frequencies of the localized defect modes were also studied, and it was observed that maximum PBG was achieved for an intermediate rotation angle of the holes. Kalra et al. [17] studied polarization-dependent PBGs (TE and TM polarizations) in 2D-PhCs with square lattices, and the results obtained suggested that PBG size is affected when the ellipticity and rotation angle of the constituent air holes/dielectric rods are changed. Liu et al. [18] proposed a double-hybrid-rods structure composed of 2D-PhCs with a square lattice, in which a square dielectric rod was connected with the slender rectangular dielectric veins in the center of each side of the dielectric square rod, and through careful adjusting of the structural parameters, the band diagram was engineered to achieve a large PBG. Hung et al. [19] demonstrated that the variation in the mid-gap frequency and PBG of elliptical PhCs against the fluctuation in the fabrication parameters indicated good tolerance to fabrication error and that the proposed patterns possessed good uniformity and high reproducibility over an area greater than $2 \times 2$ cm$^2$.

In another study by Liu et al. [20], it was demonstrated that the PBG of a 2D-PhC of a square lattice with dielectric hybrid rods in air could be tailored and optimized through rotation of the square rods and the addition of circular rods to the lattice unit cell. Wang et al. [21] reported the design of GaAs 2D-PhC with square

lattice which exhibited an absolute large PBG. It was also demonstrated that through parameter optimization, the absolute band gap of the designed structure could be improved. Furthermore, Wu et al. [22] analyzed the band gaps of a 2D-PhC with rhombic lattice and the impact of different lattice angles on the band gaps. Another type of 2D-PhC, referred to as the core-shell-type PhC, which is composed of a nanorod heterostructure array in a square or a triangular lattice, has also been studied previously [23], and it was revealed that when the nanorods were covered by other materials, PBG was considerably enhanced in size for both square and triangular lattices.

The PBG properties of a 2D-PhC based on the Thue–Morse sequence have also been studied previously [24], where it was demonstrated that by changing certain optogeometrical parameters of the structure such, as radius and refractive index, PBG of the proposed structures could be varied. Serajmohammadi et al. [25] studied the PBG properties of a 2D square lattice PhC composed of rectangular cells, and observed that the density of gaps in both TE and TM modes was high for the structure composed of rectangular dielectric rods in air, while the density was extremely low for the structure composed of rectangular air pores in a dielectric material. Furthermore, PBG properties of horizontal and vertical rectangular lattice 2D-PhC structures were studied and compared with the conventional square lattice 2D-PhC [26], where the proposed structures possessed two excellent characteristics: joint band gap regions and having band gaps at higher normalized frequencies.

More recently, by superposing two specific photonic structures with independent TE and TM band gaps, a heuristic design with complete PBG was created [27] and several innovative structures with wide complete PBGs were obtained. So far, it was shown that the band gap widths of asymmetrically-designed PhCs that consisted of square and hexagonal lattices were larger than those of symmetric ones [28]. More importantly, the largest TM band gap of the square-lattice PhCs was comparable to that of the hexagonal-lattice PhCs. In addition, the optical characteristics of a thin-film PhC that consisted of three-layer, stacked 2D PhC slabs with a structure thickness of less than a few wavelengths were theoretically analyzed with a complete PBG for both the TE and TM polarization modes [29]. It was shown that a wide PBG can be obtained in the asymmetrically-stacked PhC structure.

Several researchers have proposed engineering the photonic band gap of anisotropic photonic crystals [30–33]. Peng Shi et al. [30] reported the PBG of two-dimensional anisotropic annular photonic crystal slab structure composed of circular air holes and dielectric rods with finite thickness in a triangular lattice. Fathollahi Khalkhali et al. [31] analyzed the PBG of a square and triangular photonic crystal slabs composed of air holes in an anisotropic tellurium background with $SiO_2$ as a cladding material. The obtained results show that the proposed structures represent a full PBG with noticeable width. Further, in the paper [32], the authors indicated that a tunability of complete PBG can be obtained in both square and triangular structures with non-circular holes. The analyses of the complete PBG properties of two-dimensional dielectric-plasma photonic crystals with triangular and square lattices, composed of plasma rods with different geometrical shapes in the anisotropic tellurium background have been also presented [33].

In the above mentioned papers, the photonic band gap properties of the PhC structures were studied for different types of anisotropic PhCs with different lattices and shapes. Alternatively, silicon photonics has largely applications in near-IR data communications in the telecommunication wavelength band. Silicon material is also an optically transparent material in the wavelength range between 1.1 $\mu$m and 8 $\mu$m which can be utilized in many applications such as environmental and biochemical sensing [34]. PhC structures can be fabricated using e-beam lithography or deep UV lithography methods [35]. Both methods allow defining the circular hole patterns in a resist spun on top of the SOI wafer and induce imperfections and disorder in the fabricated PhC structures. Such disorder in the circular air–hole geometry can lead to a reduction of the PBG size and to an increase of radiation losses and thus to strongly limit the performances of PhC photonic devices [36]. Obviously, in order to avoid these problems of the fabrication and maximize the PBG, a new silicon PhC structure design with optimal structural parameters is required.

In the present study, PBG properties of silicon PhCs slab composed of elliptical, rectangular, and hexagonal air holes in triangular lattice were analyzed. The impacts of optogeometrical parameters of the proposed structures on PBG properties were analyzed using three-dimensional supercell plane-wave expansion (3D-PWE) calculations, and it was observed that the TE photonic band gap width and gap/mid-gap ratio in this silicon PhC slab exhibited oscillatory behavior with changing the rotation angle of the constituent air holes. Moreover, numerical simulations demonstrated the efficiency of the proposed silicon PhC structures for application in the design of defect mode PhC lasers, PhC nanocavities, PhC waveguides and mid-infrared sensors devices.

## 2. PhC structures design and 3D-PWE calculations

In order to analyze the PBG properties of silicon photonic crystals slab with non-circular air holes, three PhC slab structures were used. The PhCs were composed of the triangular lattice with non-circular air holes. Figure 1a depicts the model of

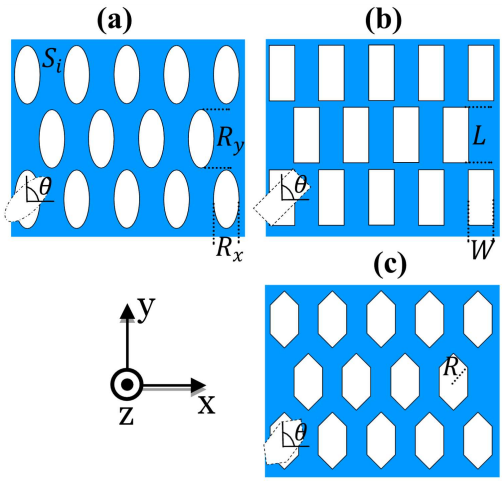


Fig. 1. Schematic configuration of photonic crystal slab consisting of a triangular lattice of (a) elliptical, (b) rectangular, and (c) hexagonal air holes. The rotating air holes in a triangular lattice, with angle $\theta$, are defined as the angle between the axis of the air holes cross-section and the lattice axis.

the PhC slab consisting of a triangular lattice with elliptical air holes, where $R_x$ and $R_y$ represented minor and major radii of the constituent elliptical holes, respectively. The ellipticity of the air holes was defined as the ratio of the major axis to the minor axis. Figure 1b depicts the model of the PhC consisting of rectangular air holes, where $L$ and $W$ represented the length and width of the constituent rectangular air holes, respectively, such that $L \leq W$. In case of this particular structure, $\beta = W/L$ represented the ratio between the width and length of the rectangles. Figure 1c illustrates the model of the PhC consisting of hexagonal air holes, where $R$ represented the side of the hexagon. In the present study, it was assumed that the periodicity of the PhC slab existed in the $X$–$Y$ plane and the rotation of the non-circular air holes relative to the lattice axes was defined by angle $\theta$. Since silicon is one of the most common materials used in the design of various devices, the materials that were used for studying the effects of the opto-geometrical parameters of the proposed structures on photonic band gaps consisted of silicon and air, especially because such structures provided adequate dielectric contrast for obtaining the photonic band gaps.

Prior to analyzing the PBG of the proposed structures, band diagram (also known as dispersion diagram) of the proposed structures was obtained using a structure composed of a silicon slab with a triangular lattice containing air holes and surrounded by air. The opto-geometrical parameters of the proposed structures have been mentioned earlier, and the slab thickness obtained was $h/a = 0.6$. Triangular lattice was used because for a slab with infinite thickness, the band gap is large for both transverse electric (TE) and transverse magnetic (TM)

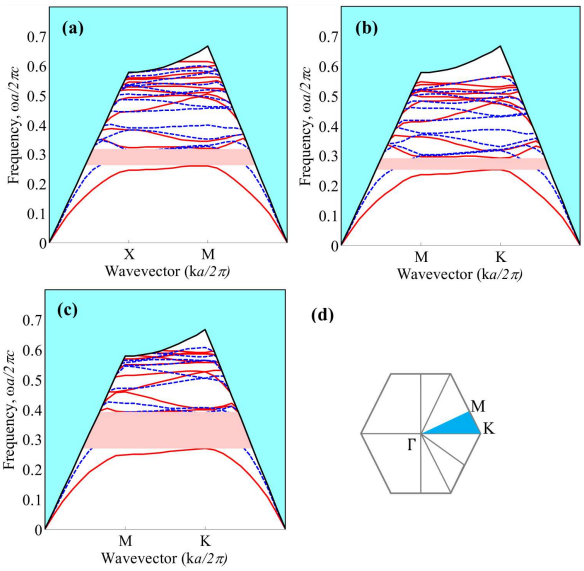


Fig. 2. (a) Band diagram for the photonic crystal slab consisting of triangular lattice of (a) elliptical, (b) rectangular, and (c) hexagonal air holes where the blue dotted line indicates the even mode, the red line indicates the odd mode, and the rectangular area indicates the photonic band gap. (d) Brillouin zone of the triangular lattice of air holes.

polarizations. Furthermore, a 2D triangular lattice with a hexagonal Brillouin zone exhibits extremely high symmetry in the plane. Therefore, within the plane of periodicity, such a structure would assist in the formation of forbidden band gaps in all the directions.

The band diagram illustrating normalized frequency versus the wave vector for the three proposed structures has been presented in Fig. 2. Band diagrams for both TE (even-modes) and TM (odd-modes) polarized modes have been depicted. The projected band diagrams of the proposed PhC structures were calculated along the Γ–$K$–$M$–Γ edge of the Brillouin zone, and the full-vectorial eigenmodes of Maxwell's equations with periodic boundary conditions were computed through preconditioned conjugate gradient minimization of the block Rayleigh quotient for a plane-wave basis, using a freely available software package [37]. In 3D-PWE calculations, supercell approach was used, with the assumption that the periodicity of the PhCs slab lies in the $X$–$Y$ plane. In order to reduce the influence of boundaries on the results, a sufficient amount of cladding material was added to the original finite height cell in the $Z$-direction as there was no periodicity in this direction. The band diagrams show a one-frequency band gap for the TE polarized modes (even-modes) but no gap for the TM modes (odd-modes), i.e., the proposed structures gives rise to a PBG for the TE-like modes in which the electric field in the centre of the PhC slab is polarized in the membrane plane. As well, in the band diagram of Fig. 2,

the fundamental band gap of the proposed structures is centered near a normalized frequency of $\omega a/2\pi c = 0.2891$, 0.2717 and 0.3294 for elliptical, rectangular and hexagon air holes, respectively.

## 3. Analyses and results

### 3.1. Elliptical air holes

The photonic band gap is extremely sensitive to variations in the critical structural parameters of PhCs slab, such as hole geometry, slab thickness, and refractive indices of the slab and the cladding materials. In the present study, two opto-geometrical parameters appeared to play an important role in determining the photonic band gap in the proposed slab structures: geometry of the constituent air holes and their rotation angles. Using the structures that were used to compute the band diagrams (Fig. 2), the effect of ellipticity of the air holes on the photonic band gap was investigated.

Figure 3 depicts the variation of TE photonic band gap width and gap/mid-gap ratio as a function of ellipticity ($\eta$) for the different values of slab thickness ($h/a$). The band gap width was determined by the frequency difference between the upper and lower edges of the TE band gap, while the gap/mid-gap ratio was calculated as the ratio between band gap width and mid-gap frequency. As observed in Fig. 3, for a particular slab thickness, there exists a large band gap width with an optimal ellipticity of holes ($\eta$). Figure 3 clearly indicates that the obtained results were qualitatively similar in terms of variations in the band gap width and gap/mid-gap ratio with an increase in the ellipticity of the holes, i.e., band gap width and gap/mid-gap ratio exhibited a considerable increase initially and decreased subsequently. For instance, for a slab thickness of $h/a = 0.4$, maximum band gap width and gap/mid-gap ratio obtained were 0.06 and 20%, respectively, for $\eta = 0.55$. Moreover, in the case depicted in Fig. 3, for a particular ellipticity of air holes, with an increase in slab thickness, photonic band gap width decreased slightly, while the gap/mid-gap ratio increase by a slight margin. Therefore, the Si slab exhibited a large band-gap width (and a low gap/mid-gap ratio) for an optimal $h$. The band gap width decreases as the slab thickness increases because for a thick slab, higher-order modes can be produced with little energy expended. Such modes lie only slightly above the lowest-order mode and stop the band gap from opening. However, a weak perturbation of the background dielectric constant occurs with a thin slab. The dispersion curve of the guided modes closely approaches the edge of the light cone and therefore becomes only weakly guided. As a result, the band gap disappears [38].

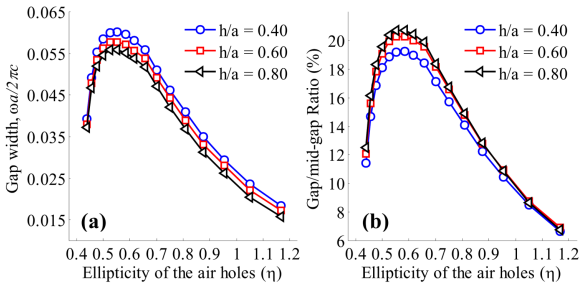


Fig. 3. Variation of (a) TE photonic band gap width and (b) gap/mid-gap ratio with the ellipticity of the air holes ($\eta$). The slab thickness is selected to be $h/a = 0.4$, 0.6 and 0.8 where $a$ is the lattice constant of the PhC slab.

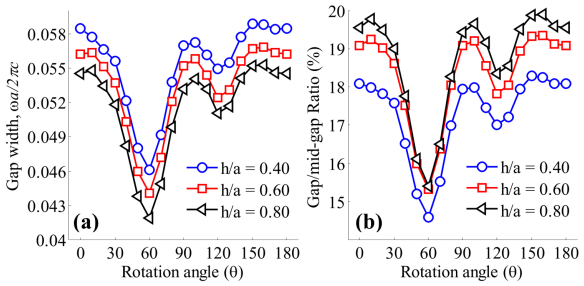


Fig. 4. Variation of (a) TE photonic band gap width and (b) gap/mid-gap ratio with the rotation angle $\theta$ of constituent elliptical air holes. The ellipticity of the air holes is $\eta = 0.5$.

Rotation of elliptical air holes is another parameter that is critical in determining the band gap. Figure 4 illustrates the variation in TE photonic band gap width and gap/mid-gap ratio as a function of rotation angle ($\theta$) of holes, for the different values of slab thickness ($h/a$). Note, that for a particular value of slab thickness, band gap width and gap/mid-gap ratio decreased with increase in the rotation angle, reached a minimum value for a particular $\theta$ value, and subsequently began to increase; a large band gap existed only for $\theta = 0°$ and $\theta = 180°$. This could be attributed to the fact that the angle of rotation would pull down additional modes below the light line, preventing the formation of the band gap. According to Fig. 4, for all the values of slab thickness, band gap width and gap/mid-gap ratio exhibited two minima at the rotation angles of $\theta = 60°$ and $\theta = 120°$. Therefore, when the rotation angle was $\theta = 60°$, the band gap for TE-like modes could be closed. The band gap could also be closed when the rotation angles reached $\theta = 120°$. However, for a fixed value of rotation angle, slab thickness did not exert a strong influence on band gap width and gap/mid-gap ratio.

### 3.2. Rectangular air holes

A similar analysis as mentioned above was performed for the second structure as well, i.e. the PhC slab composed of rectangular air holes, as depicted in Fig. 1b, using the 3D-PWE method. Firstly,

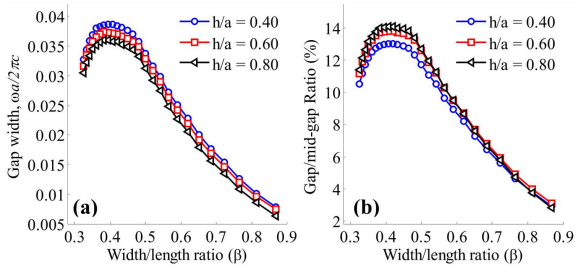


Fig. 5. Variation of (a) TE photonic band gap width and (b) gap/mid-gap ratio with the width to length ratio $\beta$. The slab thickness is selected to be $h/a = 0.4$, 0.6, and 0.8.

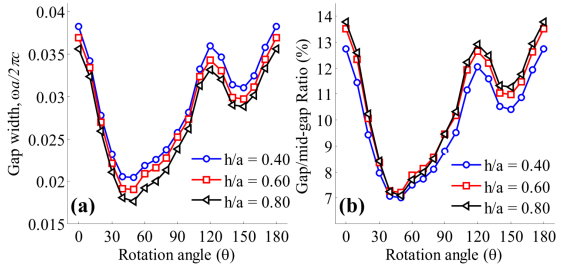


Fig. 6. Variation of (a) TE photonic band gap width and (b) gap/mid-gap ratio with the rotation angle $\theta$ of constituent rectangular air holes. The width to length ratio is $\beta = 0.371$.

the impact of the width to length ratio of the rectangles $\beta$ on band gap width and gap/mid-gap ratio was studied. In this case, slab thickness was an adjustable parameter. Therefore, photonic band gap of the structure was investigated for all the possible values of $\beta$, when a reasonable and fixed value was selected for slab thickness. Figure 5 illustrates the variation of TE photonic band gap width and gap/mid-gap ratio as a function of ratio $\beta$ of the constituent rectangular air holes. Similar qualitative behavior for band gap width and gap/mid-gap ratio was observed in this structure as well, i.e. for all the values of slab thickness, band gap width and gap/mid-gap ratio increased initially with an increase in ratio of $\beta$, became maximum for a particular value of $\beta$, and began decreasing thereafter. In fact, comprehensive investigations have demonstrated that a large PBG appears in such structures if the opto-geometrical parameter $\beta$ is in the range of 0.35 and 0.50. It should be noted that the maximum band gap width was achieved at $\beta = 0.4$ for all the values of slab thickness. Figure 5 also indicated that as the width of the rectangles approached their length, PBG was nearly closed.

Subsequently, the effect of the rotation angle of the rectangular air holes on band gap width and gap/mid-gap ratio was analyzed. In this case, ratio $\beta$ of the rectangular air holes was kept constant, and slab thickness was treated as an adjustable parameter. Figure 6 illustrates the variation of TE photonic band gap width and gap/mid-gap ratio as a function of the rotation angle of the constituent rectangular air holes for the three different values of slab thickness, i.e. $h/a = 0.4$, 0.6, and 0.8. Results similar to those obtained for the previously studied structures were obtained, i.e. for a particular value of slab thickness, band gap width and gap/mid-gap ratio of the structure decreased with increase in the rotation angle of the rectangular air holes, reached a minimum value for a particular $\theta$ value, and thereafter began increasing again. The results obtained were, therefore, compatible with the previously obtained results. The photonic band gap width and gap-mid-gap ratio exhibited two minima at $\theta = 45°$ and $\theta = 145°$ when the slab thickness ranged from $0.4a$ to $0.8a$.

### 3.3. Hexagonal air holes

Finally, change in the PBG of the PhC slab with hexagonal air holes was analyzed. Unlike the previous analyses, in this subsection, the effects of the hexagon side $R$ and their angles of rotation on photonic band gap width and gap/mid-gap ratio were studied. At first, the analysis focused on the effect of the hexagon side. Similar to previous structures, photonic band gap width and gap/mid-gap ratio of the structures were investigated for all the possible values of $R$ associated with the three values of slab thickness. As observed from Fig. 7, the TE photonic band gap width and gap/mid-gap ratio increased initially with increasing $R$, became maximum, and decreased thereafter, for all the values of slab thickness. In brief, the findings may be summarized as follows: firstly, as depicted in Fig. 7, for all the values of slab thickness, a large band gap appeared for $R = 0.38$, for which the gap/mid-gap ratio was approximately 37%. Therefore, for this structure, the effect of hexagon side on the band gap was different from the effect of ellipticity and that of the rectangular air holes studied in the previous structures, because in this case, the photonic band gap width and gap/mid-gap ratio increased initially, followed by a decrease. Secondly, the slab thickness did not exert a great impact on the photonic band gap width and gap/mid-gap ratio when the hexagon side $R$ was maintained at a constant level. The graphs indicated that increasing the slab thickness led to a slight increase in the band gap width.

In addition, the impact of rotation angle of the hexagonal air holes on photonic band gap width and gap/mid-gap ratio was analyzed. In this case, slab thickness could be varied to optimize the photonic band gap. The results obtained are presented in Fig. 8. As observed in Fig. 8, post 180° rotation of the hexagonal air holes, the structure exhibited the same photonic band gap width as it exhibited at the beginning of the analysis. In fact, for all the values of slab thickness, both band gap width and gap/mid-gap ratio exhibited an oscillatory behavior with a period of 60°. Comprehensive investigations revealed that when $\theta$ angles were in the range of 0° and 180°, photonic band gap width

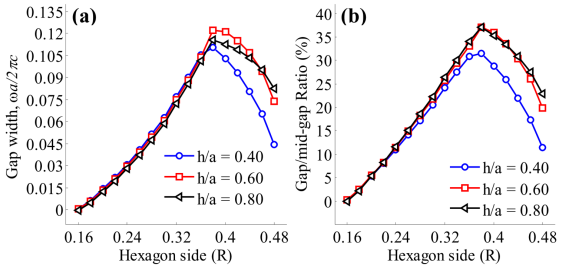


Fig. 7. Variation of (a) TE photonic band gap width and (b) gap/mid-gap ratio with the hexagon size $R$. The slab thickness is selected to be $h/a = 0.4$, 0.6 and 0.8.

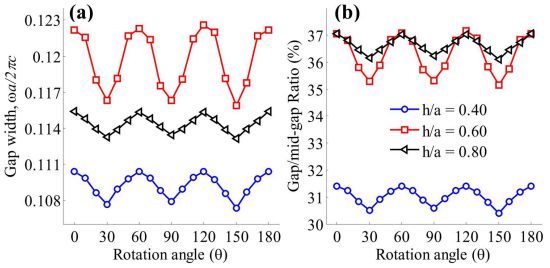


Fig. 8. Variation of TE photonic band gap width and gap/mid-gap ratio with the rotation angle $\theta$ of constituent hexagonal air holes. The hexagon side is $R = 0.36$.

and gap/mid-gap ratio curves presented three minima at $\theta = 30°$, 90°, and 150°, and a large photonic band gap width could be observed only at $\theta = 0°$, 60°, and 120°. These results appeared to be due to the base of symmetry considerations.

Until now, theoretical and experimental studies on PhC have almost exclusively concentrated on a triangular lattice of circular air holes etched in silicon PhC slab. In this study, silicon PhC structures consist of arrays of non-circular air holes in a triangular lattice is proposed and analyzed. From the above analysis, we conclude that the PBG depends mainly on the shape of the constituent air holes and their rotation angle. It has been shown that with the proper design of the shape of the constituent objects, the position and size of PBG in a PhC can be engineered to meet the requirements of the specific applications. This study set out to determine that silicon PhC with a triangular lattice of hexagonal air holes has a large PBG in even modes as their circular counterpart. By increasing the filling factor, we can thus obtain absolute PBG in guided modes situated at higher frequencies in the band diagram. Such structure added some flexibility in design and can prove helpful in the design of the photonic band gap-based devices. Since the etch-depth of the circular air holes are finite in the $SiO_2$ layer, the major fabrication challenge for the realization of PhC structures is that the realistic implementations are prone to idealities, including distortions to the hole shape or positioning which can be introduced in the fabrication process. Therefore, the experimental realization of our proposed silicon PhC structures is generally technically achievable with classical nanofabrication techniques, such as electron-beam lithography followed by reactive ion etching [35]. We believe that the results of this work will be valuable for understanding the influence of the design parameters on the PBG proprieties of the silicon PhC structures with non-circular air holes, and for designing high-quality factor PhC nanocavities and low loss PhC waveguides.

## 4. Conclusion

The present study performed a detailed analysis of photonic band gap properties of the triangular lattices with elliptical, rectangular, and hexagonal air holes in silicon photonic crystal slab. Extensive calculations utilizing 3D-PWE method revealed that PBG depends on mid-gap frequency, which in turn depends on the ellipticity, rectangularity, and hexagonality of the constituent air holes and on their rotation angles. The results of the present study revealed that the proposed structures presented a large band gap width and gap/mid-gap ratio for the optimum values of structural parameters. The maximum band gap was obtained for the triangular lattice with hexagonal air holes, a structure that exhibited a band gap width nearly 3 times larger than that of the structures composed of elliptical and rectangular air holes. The photonic band gap analysis of the structures proposed in the present study may be able to assist in designing various silicon PBG devices, such as cavities, waveguides, sensors, and splitter, where the existence of a large PBG is required to allow strong photon localization within the gap and a detailed manipulation of photonic defect states. In addition, the results of the present study may assist in designing novel coupled-cavity waveguides, the properties of which could be tuned by using rotated elliptical, rectangular, or hexagonal holes instead of circular holes.

## References

[1] E. Yablonovitch, *Phys. Rev. Lett.* **58**, 2059 (1987).

[2] J. Sajeev, *Phys. Rev. Lett.* **58**, 2486 (1987).

[3] J.D. Joannopoulos, S.G. Johnson, J.N. Winn, R.D. Meade, *Molding the Flow of Light*, Princeton Univ. Press, Princeton (NJ) 2008.

[4] O. Painter, R.K. Lee, A. Scherer, A. Yariv, J.D. O'Brien, P.D. Dapkus, I. Kim, *Science* **284**, 1819 (1999).

[5] A. Mekis, J.C. Chen, I. Kurland, Shanhui Fan, P.R. Villeneuve, J.D. Joannopoulos, *Phys. Rev. Lett.* **77**, 3787 (1996).

[6] L. Kassa-Baghdouche, T. Boumaza, M. Bouchemat, *Physica Scr.* **90**, 065504 (2015).

[7] L. Kassa-Baghdouche, T. Boumaza, M. Bouchemat, *Appl. Phys. B* **121**, 297 (2015).

[8] L. Kassa-Baghdouche, T. Boumaza, E. Cassan, M. Bouchemat, *Optik* **126**, 3467 (2015).

[9] L. Kassa-Baghdouche, T. Boumaza, M. Bouchemat, *Opt. Eng.* **53**, 127107 (2014).

[10] L. Kassa-Baghdouche, *Physica Scr.* **95**, 015502 (2019).

[11] L. Kassa-Baghdouche, E. Cassan, *Opt. Quant. Electron.* **51**, 328 (2019).

[12] L. Kassa-Baghdouche, E. Cassan, *Photon. Nanostruct. Fundament. Appl.* **28**, 32 (2018).

[13] L. Kassa-Baghdouche, E. Cassan, *Instrumentat. Sci. Technol.* **46**, 534 (2018).

[14] L. Kassa-Baghdouche, E. Cassan, *Opt. Quant. Electron.* **52**, 260 (2020).

[15] L. Kassa-Baghdouche, *J. Opt. Soc. Am. B* **37**, A277 (2020).

[16] A. Matthews, S. Mingaleev, Y. Kivshar, *Laser Phys.* **14**, 631 (2004).

[17] Y. Kalra, R.K. Sinha, *Pramana* **67**, 1155 (2006).

[18] Wen-Long Liu, Tzong-Jer Yang, *Phys. Lett. A* **369**, 518 (2007).

[19] Yung-Jr Hung, San-Liang Lee, Yen-Ting Pan, *J. Opt.* **12**, 015102 (2009).

[20] Wen-Long Liu, Yeuh-Yeong Liou, Jung-Chun Wei, Tzong-Jer Yang, *Physica B Condens. Matter* **404**, 4237 (2009).

[21] Donglin Wang, Zhongyuan Yu, Yumin Liu, Pengfei Lu, Lihong Han, Hao Feng, Xiaotao Guo, Han Ye, *Opt. Expr.* **19**, 19346 (2011).

[22] Zhenhai Wu, Kang Xie, Huajun Yang, *Optik* **123**, 534 (2012).

[23] Dan Liu, Yihua Gao, Dingshan Gao, Xiangyun Han, *Opt. Commun.* **285**, 1988 (2012).

[24] F. Mehdizadeh, H. Alipour-Banaei, *J. Opt. Commun.* **34**, 61 (2013).

[25] S. Serajmohammadi, H. Alipour-Banaei, *Frontiers Optoelectron.* **6**, 346 (2013).

[26] H. Alipour-Banaei, S. Serajmohammadi, F. Mehdizadeh, A. Andalib, *J. Opt. Commun.* **36**, 109 (2015).

[27] Fei Meng, Shuo Li, Yang Fan Li, Baohua Jia, Xiaodong Huang, *Mater. Lett.* **207**, 176 (2017).

[28] Fei Meng, Yangfan Li, Shuo Li, Han Lin, Baohua Jia, Xiaodong Huang, *J. Lightwave Technol.* **35**, 1670 (2017).

[29] Se-Young Park, Heungjoon Kim, Bong-Shik Song, *Opt. Expr.* **26**, 29521 (2018).

[30] Peng Shi, Kun Huang, Xue-Liang Kang, Yong-Ping Li, *Opt. Expr.* **18**, 5221 (2010).

[31] T. Fathollahi Khalkhali, B. Rezaei, A. Soltani Vala, M. Kalafi, *Appl. Opt.* **52**, 3745 (2013).

[32] T. Fathollahi Khalkhali, A. Bananej, *Opt. Commun.* **369**, 79 (2016).

[33] T. Fathollahi Khalkhali, A. Bananej, *Phys. Lett. A* **380**, 4092 (2016).

[34] R. Soref, *Nature Photon.* **4**, 495 (2010).

[35] P.I. Borel, L.H. Frandsen, A. Harpoth, M. Kristensen, T. Nemi, Pengfei Xing, J.S. Jensen, O. Sigmund, in: *Proc. 2004 6th Int. Conf. on Transparent Optical Networks, IEEE Cat. No. 04EX804 Vol. 1, Wroclaw (Poland) 2004*, IEEE, 2004, p. 271.

[36] R. Ferrini, D. Leuenberger, R. Houdré, H. Benisty, M. Kamp, A. Forchel, *Opt. Lett.* **31**, 1426 (2006).

[37] S. Johnson, J. Joannopoulos, *Opt. Expr.* **8**, 173 (2001).

[38] S.G. Johnson, Shanhui Fan, P.R. Villeneuve, J.D. Joannopoulos, L.A. Kolodziejski, *Phys. Rev. B* **60**, 5751 (1999).